Electronic Supplementary Information

Synthesis of Large-sized Gold Nanoparticles with Deformation Twinnings by One-step Seeded Growth with Cu(II)-mediating Oswald Ripening for Determining Nitrile and Isonitrile Group

Chenshuo Wu,[a] Hongpeng He, [a] Yahui Song, [a] Cuixia Bi, [a] Lixiang Xing,[a] Wei Du,[b] Shenggang Li,[c] and Haibing Xia [a,]*

[a.] State Key Laboratory of Crystal Materials, Shandong University, Jinan, 250100, P. R. China. E-mail: hbxia@sdu.edu.cn
[b.] School of Environment and Material Engineering, Yantai University, Yantai 264005, Shandong, China.
[c.] CAS Key Laboratory of Low-Carbon Conversion Science and Engineering, Shanghai Advanced Research Institute, Chinese Academy of Sciences, 100 Haike Road, Shanghai 201210, China.

Figure S1. TEM images (a to g) of differently-sized quasi-spherical (QS) Au NPs with a single crystalline structure obtained by one-step seeded growth method in the absence of Cu^{2+} ions: 13 nm (a), 20 nm (b), 28 nm (c), 38 nm (d), 48 nm (e), 61 nm (f), and 70 nm (g). The SAED pattern (h) of one individual 70 nm QS Au NP.

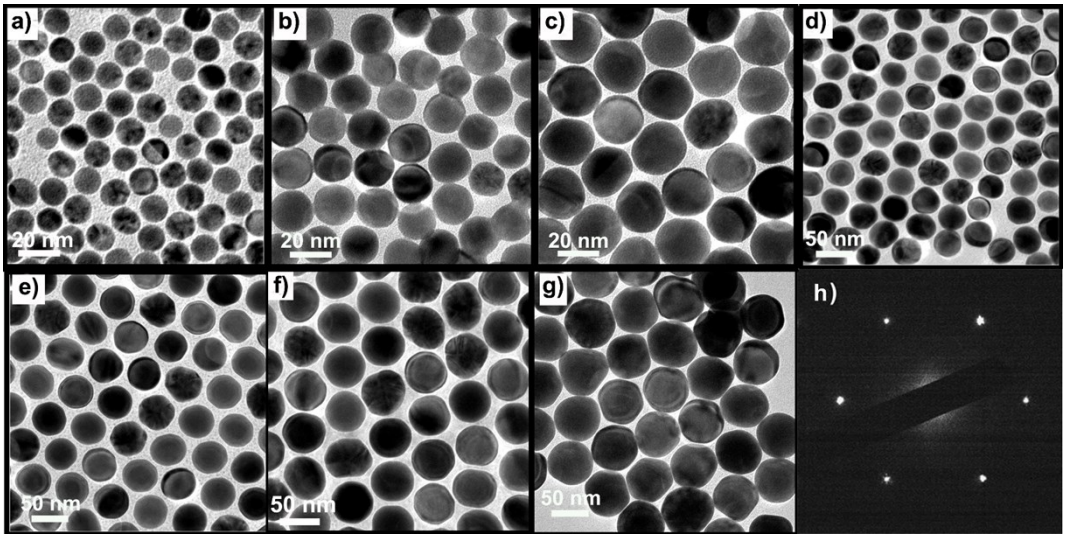

The synthetic procedure of quasi-spherical (QS) Au NPs with average diameters from 13 to 70 nm is the same as that of large-sized QS Au NPs with average diameters from 70 to 196 nm, except the absence of Cu^{2+} ions. The detail recipes are listed in Table S1.

As shown in Figure S1, QS Au NPs with average diameters from 13 to 70 nm were successfully synthesized by the one-step seeded growth method in the absence of Cu^{2+} ions. They have a narrow distribution in shape and size. In addition, the standard deviations and ellipticities of the as-prepared Au NPs were calculated to be less than 6% and 1.06, respectively (Table S2). Moreover, the selected area electron diffraction (SAED) pattern of one individual QS Au NP (Figure S1h) indicates the as-prepared QS Au NPs have single crystalline structure (QS Au_s NPs).

Figure S2. Extinction spectra of QS Au NPs with average diameters from 13 to 70 nm obtained by one-step seeded growth method in the absence of Cu^{2+} ions. The inset in (a) is the photographs of the aqueous dispersions of the corresponding QS Au_s NPs. (b) Extinction spectra of Au NPs with a perfect spherical shape calculated on the basis of Mie theory with the same sizes and standard deviation rates as the corresponding QS Au_s NPs obtained experimentally.

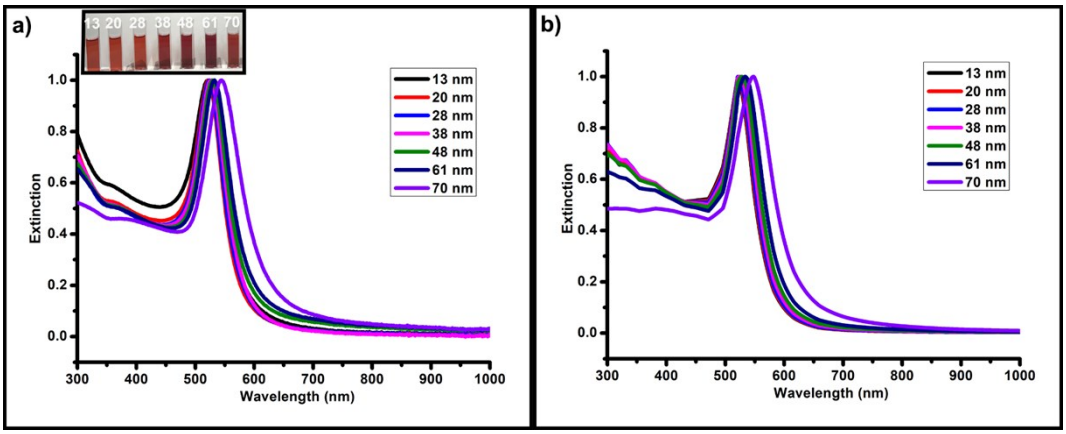

As shown in Figure S2a, it clearly found that with their average diameters increasing, the center positions of the dipolar surface plasmon resonance (SPR) peaks of the as-prepared QS Au NPs gradually red-shift to the longer wavelength, which is consistent with their size-dependent optical properties. For instance, when the average diameter increases from 13 to 70 nm, the center position of their dipolar SPR peaks gradually red-shift from 521 to 548 nm. In addition, the as-prepared QS Au NPs exhibit the rather symmetric dipolar SPR peaks with a narrow half-width, and no nonzero baselines at longer wavelengths are observed (>700 nm). The results illustrate that Au NPs with average diameters ranging from 13 to 70 nm are monodispersed and bear a quasi-spherical shape. The continuous red-shift in the center positions of the SPR peaks of the as-prepared QS Au NPs with the increasing NP diameters is also clearly reflected in the variation of the color of their aqueous dispersions (inset in Figure S2a). According to their average diameters and the standard size deviations, the extinction spectra of the as-prepared Au NPs are calculated by the Mie theory and showed in Figure S2b. One can clearly see that the experimental extinction spectra are consistent with the ones calculated from Mie theory (Figure S2 and Table s2). The results indicate that the as-prepared Au NPs have a good quasi-spherical shape and have a narrow size distribution (as shown in the TEM images in Figure S1).

Figure S3. TEM images of 3 nm Au-NP seeds.

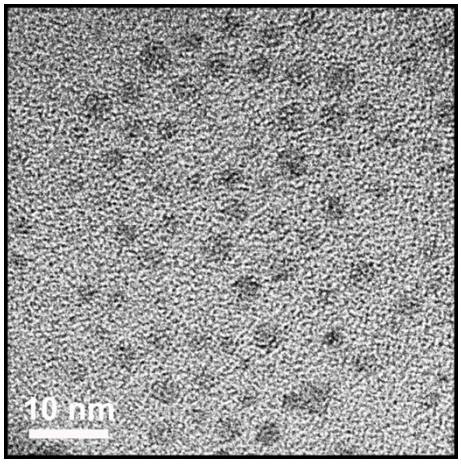

Figure S4. TEM images of Au NPs obtained in the presence of different concentrations of Cu^{2+} ions: 0.5 μM (a), 1 μM (b), 2 μM (c), and 4 μM (d), respectively. The concentrations of $HAuCl_4$ and AA are fixed at 2.5 μM and 5.0 μM, respectively. And the particle number of 3 nm Au-NP seeds is 1.56×10^{10} constantly.

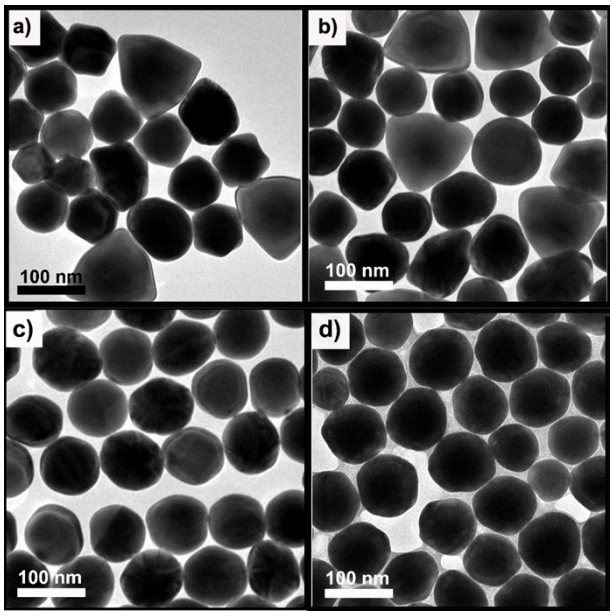

In our one-step seeded growth method with Cu^{2+}-mediating Ostwald ripening, the concentration of Cu^{2+} ions is essential for the formation of uniform Au NPs in shape and size. For example, the recipe for the preparation of 70 nm Au NPs is the same but the concentrations of Cu^{2+} ions is changed from 0.5 to 1, 2, and 4 μM, the shapes, average diameters and size distribution of the final Au NPs are varied (Figure S4). The optimal concentration of Cu^{2+} ions for the synthesis of QS Au NPs with a narrow size distribution is about 2 μM (Figure S4c).

Figure S5. TEM images of Au NPs obtained in the absence of Cu^{2+} ions. The concentrations of $HAuCl_4$ and AA are fixed at 2.5 μM and 5 μM, respectively. And the particle number of Au-NP seeds for (a) and (b) is 2.1×10^9 and 5.2×10^8, respectively.

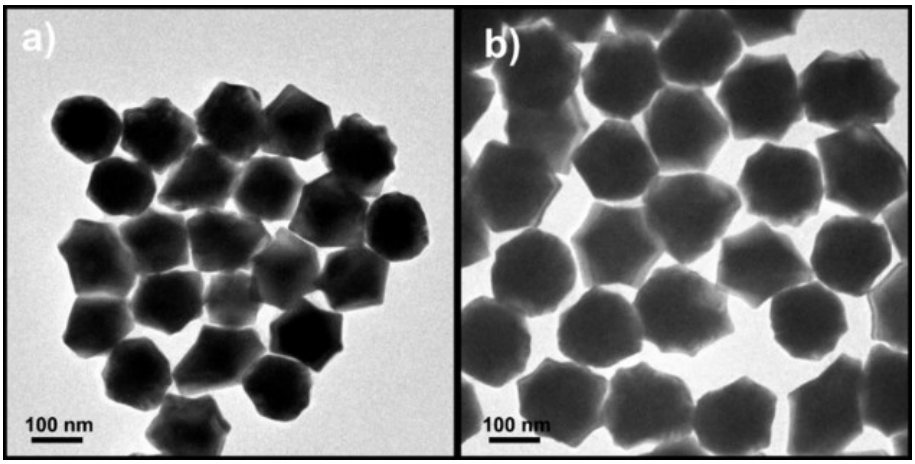

Figure S6. TEM images of Au NPs obtained in the presence of different concentrations of Cu^{2+} ions: 0.02 μM (a), 0.04 μM (b), 0.1 μM (c), and 0.2 μM (d), respectively. The concentrations of $HAuCl_4$ and AA are fixed at 2.5 μM and 5.0 μM, respectively. And the particle number of 3 nm Au-NP seeds is 2.1×10^9 constantly.

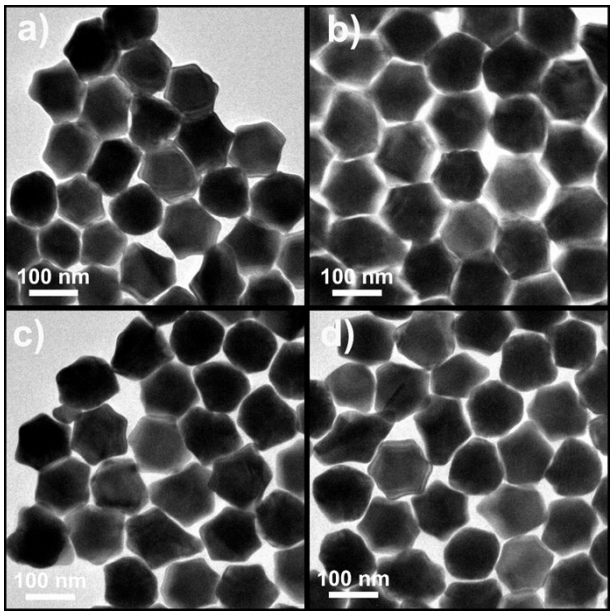

In our one-step seeded growth method with Cu^{2+}-mediating Ostwald ripening, the concentration of Cu^{2+} ions is essential for the formation of uniform TOH Au NPs in shape and size. For example, the recipe for the preparation of 70 nm TOH Au NPs is the same but the concentrations of Cu^{2+} ions is changed from 0.02 to 0.04, 0.1 and 0.2 μM, the shapes, average diameters and size distribution of the final TOH Au NPs are varied (Figure S6). The optimal concentration of Cu^{2+} ions for the synthesis of QS Au NPs with a narrow size distribution is about 0.04 μM (Figure S6b).

Figure S7. The geometrical model of a single TOH NP viewed along the <110> direction.

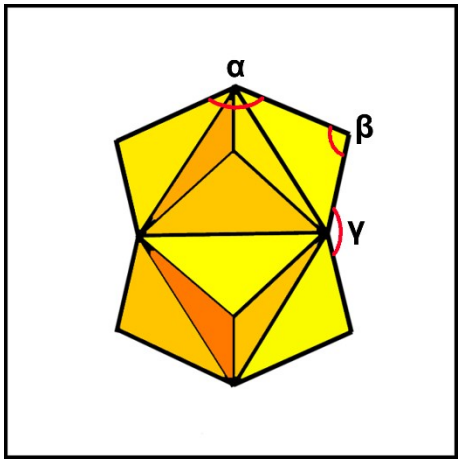

Figure S8. Comparison between extinction spectra of {331}-faceted TOH NPs with average diameters of 140 nm (a) and 195 nm (b) obtained by our one-step seeded growth method with Cu^{2+}-mediating Ostwald ripening (solid lines) and those with the comparable size obtained by our multi-step seeded growth method (dashed lines).

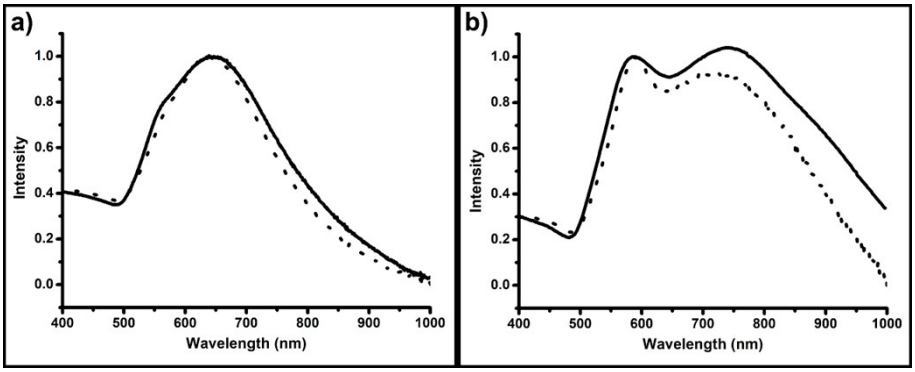

The high quality {331}-faceted TOH NPs with average diameters of 140 nm and 195 nm have been synthesized by the multi-step seeded growth method in our previous work.[1] By contrast, the extinction spectra of the as-prepared TOH Au NPs in this work are rather similar to those with the comparable size in our previous work. This result indicate that our one-step seeded growth method with Cu^{2+}-mediating Ostwald ripening indeed can fabricate high quality TOH Au NPs.

Figure S9. TEM images of the amount of Au nuclei during the synthesis of TOH Au NPs (a and b) and QS Au NPs (c and d), which were taken out at different reaction times: 60 s (a, c) and 10 min (b, d). The recipes for synthesis of TOH Au NPs and QS Au NPs are the same except the concentrations of Cu^{2+} ions: 0.04 μM for TOH Au NPs (a and b), and 2 μM for QS Au NPs (c and d), respectively. The concentrations of $HAuCl_4$ and AA were fixed at 2.5 μM and 5 μM, respectively. The particle number of 3 nm Au-NP seeds were all 2.1×10^9.

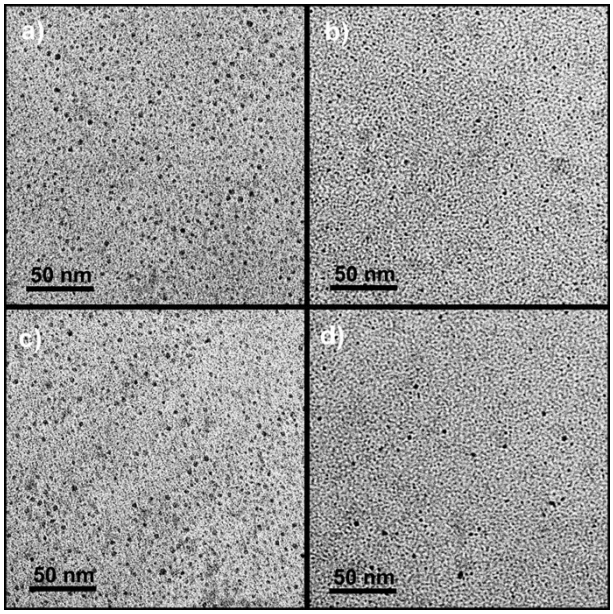

Figure S10. TEM images of one individual TOH Au NPs with average diameters of 70 nm viewed along <110> direction (a), and TOH Au NPs in an orderly arrangement (b). The resulting TOH Au NPs were prepared according to our previous work.[1]

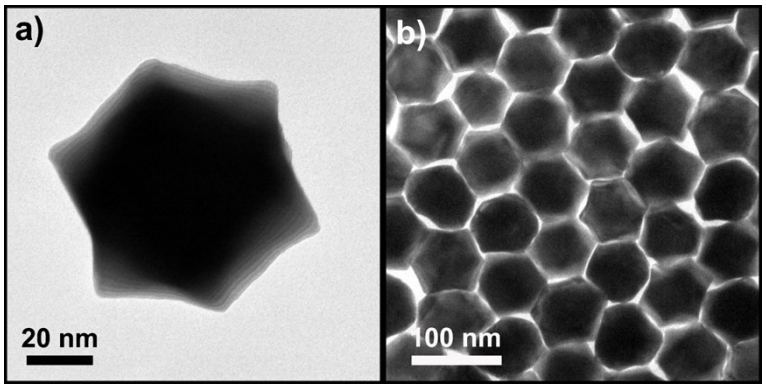

Figure S11. Optical images of glass substrate coated with QS Au NPs (a) and glass substrate coated with TOH Au NPs (b).

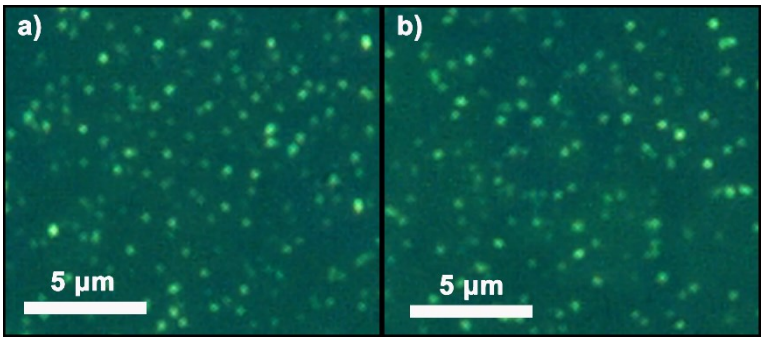

Thanks to their special chromatic dispersion, these Au NPs can be observed as bright spots by optical microscope, which can represent the distribution of the Au NPs on the glass substrates. As such, the observed distribution of NPs coated on glass substrates will be consistent with that used for SERS tests. Thus, digital images obtained by the Raman microscope was selected to characterize the distribution of NPs coated on glass substrates. After several rounds of attempts, the eligible SERS substrates were obtained by using a rather diluted dispersion of Au NPs, on which there is hardly any NP aggregates (Figure S11). After the successful preparation of the eligible SERS substrates, the SERS spectra of different concentrations of CV probes adsorbed on the as-prepared SERS substrates were investigated and their corresponding enhancement factors (EFs) were calculated accordingly.

Figure S12. The Raman signal of CV probes on the blank glass substrate. The excitation laser wavelength for Raman measurements is 633 nm. The acquisition time is 10 s, and the laser power is 0.1 mW.

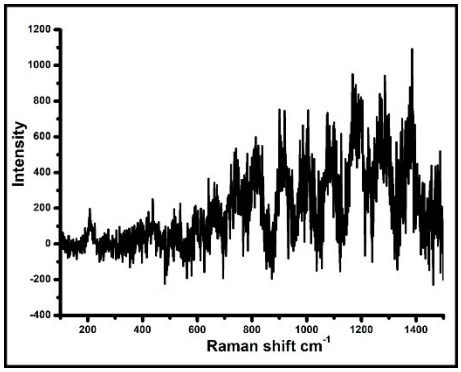

The calculation of the enhancement factor (EF) based on the following equations from (1) to (3):[2,3]

$$EF = \frac{I_{SERS} N_{normal}}{I_{normal} N_{SERS}} \quad (1)$$

where I_{SERS} is the intensity of a specific band of the probes in the SERS spectra; I_{normal} is the intensity of the same band of the probes in the normal Raman spectra under the same conditions (Table S4); N_{normal} is the number of probe molecules in the excitation volume for the normal Raman measurements; and N_{SERS} is the total number of adsorbed molecules on the Au NPs in the excitation volume contributing to I_{SERS}.

In our case, CV is chosen as the probes for the *EF* calculations and the specific band is 210 cm^{-1}. The N_{normal} is estimated by using the following equations:

$$V = \pi\left(\frac{d}{2}\right)^2 H \quad (2)$$

$$N_{normal} = \left(\frac{VD}{M}\right) N_A \quad (3)$$

where d is the diameter of the beam size (d = 1.5 μm) and H is the effective depth of focus (H = 2 μm, which was estimated by finely controlling the height of the stage during the Raman measurements). D is the density of CV probes (1.19 g/mL), M is the molar mass of CV probes (407.99 g/mol), and $N_A = 6.02 \times 10^{23}$ mol^{-1} is the Avogadro constant.

To estimate the N_{SERS}, it is known that the first monolayer gives the largest contribution to SERS spectra,[4,5] therefore we assumed that the CV molecules were adsorbed as a closely packed monolayer with a molecular footprint of 1.51 nm^2.[4,6,7] The surface area of one QS and one TOH Au NP can be estimated by the corresponding calculation (πD^2 for QS Au NPs and $7.09D^2$ for TOH Au NPs, in which D is the diameter of the QS- or TOH Au NP), respectively. Based on the surface density of Au NPs on the glass substrate (7.6×10^6 particles/mm^2) and the diameter of the beam size (d = 1.5 μm), the average particle number of the Au NPs in the excitation volume can be estimated as 13. Therefore, their EFs are estimated accordingly.[3]

The standard deviations in intensity of the specific mode were determined by the multiple measurements. Error bars are then presented on EF graphs.

Figure S13. Representative SERS signals of different concentrations of CV probes adsorbed on the glass substrate coated with 70 nm QS Au NPs with a rough surface: 10^{-3} M (a), 10^{-5} M (b), 10^{-6} M (c), 10^{-7} M (d), 10^{-8} M (e) and 10^{-9} M (f). The excitation laser wavelength for Raman measurements is 633 nm. The acquisition time is 10 s, and the laser power is 0.1 mW.

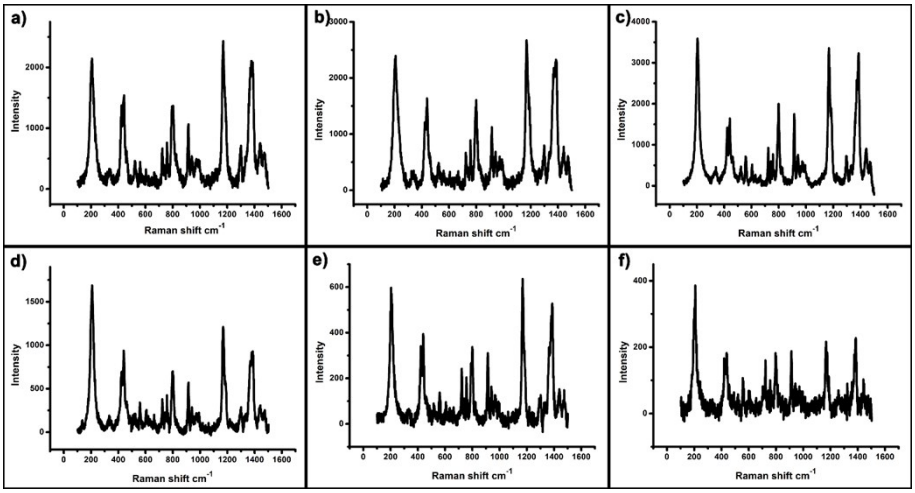

Figure S14. Representative SERS signals of different concentrations of CV probes adsorbed on the glass substrate coated with 70 nm TOH Au NPs with sharp tips: 10^{-3} M (a), 10^{-5} M (b), 10^{-6} M (c), 10^{-7} M (d), 10^{-8} M (e) and 10^{-9} M (f). The excitation laser wavelength for Raman measurements is 633 nm. The acquisition time is 10 s, and the laser power is 0.1 mW.

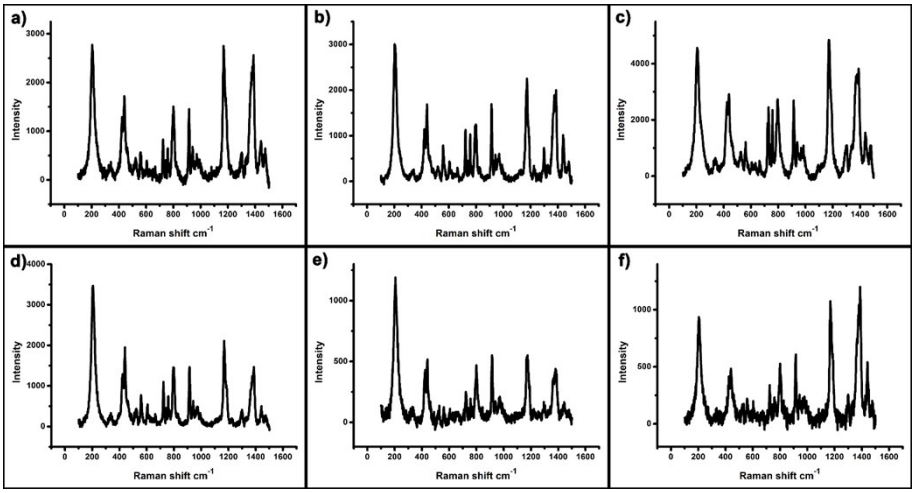

Figure S15. (a) SERS spectra of QS Au NPs solely absorbed with CV probes (10^{-5} M) (black curve) and QS Au NPs absorbed with CV probes (10^{-5} M) and 4-ATP probes (10^{-7} M) (red curve). (b) SERS spectra of TOH Au NPs solely absorbed with CV probes (10^{-5} M) (black curve) and TOH Au NPs absorbed with CV probes (10^{-5} M) and 4-ATP probes (10^{-7} M) (red curve). (c) SERS spectra of TOH Au NPs solely absorbed with CV probes (10^{-7} M) (black curve) and TOH Au NPs absorbed with CV probes (10^{-7} M) and 4-ATP probes (10^{-7} M) (red curve). The excitation laser wavelength is 633 nm, the laser power is 0.1 mW, and the acquisition time is 10 s.

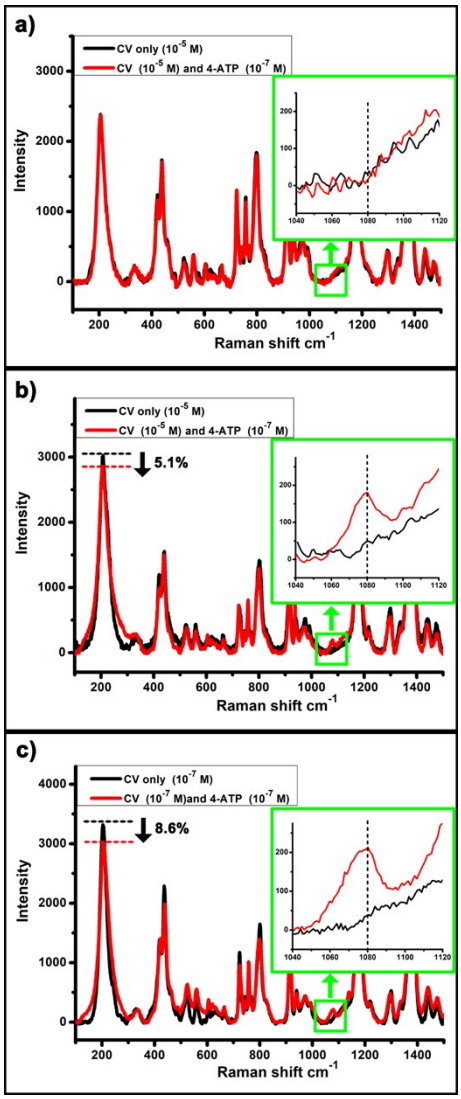

Three groups of control experiments were conducted and the detailed experimental procedure was as follows. a) SERS spectra of QS Au NPs absorbed with CV probes (10^{-5} M) and TOH Au NPs absorbed with CV probes (10^{-5} M and 10^{-7} M) were firstly tested (black curves in Figure S15). b) Then, QS Au NPs absorbed with CV probes (10^{-5} M) and TOH Au NPs absorbed with CV probes (10^{-5} M and 10^{-7} M) were further treated to absorb 4-ATP probes (10^{-7} M). c) Lastly, SERS spectra of QS Au NPs absorbed with CV probes and 4-ATP probes, and TOH Au NPs absorbed with CV probes and 4-ATP probes were tested (red curves in Figure S15).

In the SERS spectra of QS Au NPs absorbed with CV probes (10^{-5} M) and 4-ATP probes (10^{-7} M), the characteristic peak of 4-ATP probes (at 1080 cm^{-1}) is not observed. Moreover, the intensity

of the characteristic peak of CV probes (at 210 cm^{-1}) is nearly the same to that in the SERS spectra of QS Au NPs solely absorbed with CV probes (10^{-5} M) (Figure S15a). The results indicating that no CV probes were replaced by 4-ATP probes. However, in the SERS spectra of TOH Au NPs absorbed with CV probes (10^{-5} M) and 4-ATP probes (10^{-7} M), the distinct characteristic peak of 4-ATP probes (at 1080 cm^{-1}) appears while the characteristic peak of CV probes (at 210 cm^{-1}) showed a small decrease of ~5.1% in the intensity (Figure S15b), compared with that of TOH Au NPs solely absorbed with CV probes (10^{-5} M). In addition, in the SERS spectra of TOH Au NPs absorbed with CV probes (10^{-7} M) and 4-ATP probes (10^{-7} M), the distinct characteristic peak of 4-ATP probes (at 1080 cm^{-1}) still appears while the characteristic peak of CV probes (at 210 cm^{-1}) showed a small decrease of ~8.6% in the intensity (Figure S15c), compared with that of TOH Au NPs solely absorbed with CV probes (10^{-7} M). One can conclude that physically-adsorbed CV probes of high concentration (10^{-5} M) on QS Au NPs cannot be replaced by chemically-adsorbed 4-ATP probes (10^{-7} M). However, physically-adsorbed CV probes of high concentration (10^{-5} M) on TOH Au NPs can be replaced by chemically-adsorbed 4-ATP probes of low concentration (10^{-7} M). Moreover, chemically-adsorbed 4-ATP probes only can replace a small portion of physically-adsorbed CV probes adsorbed on TOH Au NPs and most of physically-adsorbed CV probes are still adsorbed on TOH Au NPs.

It is known that the stability of chemically-adsorbed probes on the sharp tips of TOH Au NPs should be better than that of physically adsorbed probes because sharp tips bear high surface energy.[8-10] Thus, physically-adsorbed CV probes adsorbed on sharp tips of TOH Au NPs can be replaced by chemically-adsorbed 4-ATP probes of the same concentration. On the basis of the above results, only CV probes adsorbed on sharp tips of TOH Au NPs can be replaced by 4-ATP probes. Therefore, physically-adsorbed CV probes may mainly adsorb on the flat surfaces of TOH Au NPs with sharp tips and a small fraction of them adsorb on their sharp tips.

Figure S16. Schematic illustration of the adsorption geometry of the nitrile group bonds to metal atom in the atop configuration (a); and that of the isonitrile group bonds to metal atoms in the atop, and hollow configurations (b), respectively.

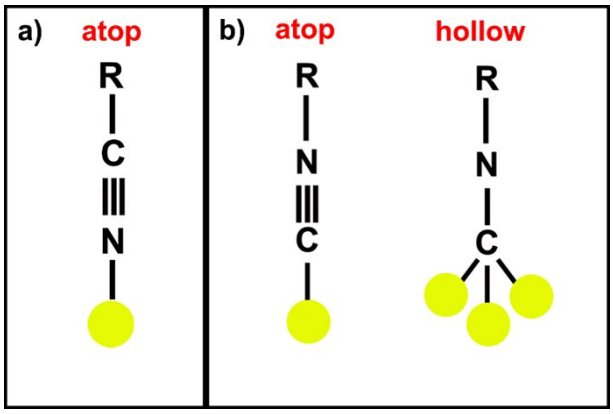

Figure S17. Evolution of UV-visible spectra of 4-nitrophenol (4-NP) ring the reduction by $NaBH_4$, which were recorded at different reaction time intervals. Since the catalytic reaction started in the presence of Au_s-Pd NPs (a) and Au_{dt}-Pd NPs (b), the corresponding plots of $\ln(A/A_0)$ against the reaction time of the reduction of 4-NP are shown in (c).

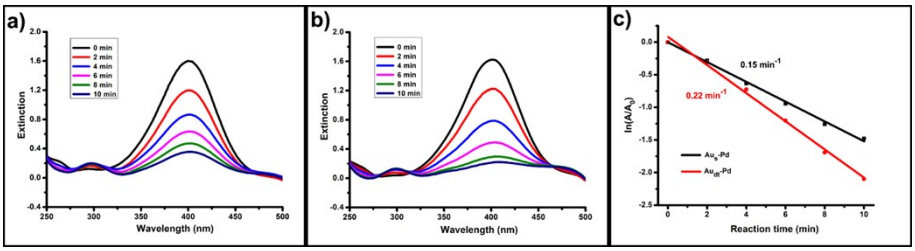

The as-prepared 70 nm QS Au NPs with a single crystalline structure (QS Au_s NPs) (Figure S2g) and 70 nm QS Au NPs with deformation twinning (QS Au_{dt} NPs) (Figure 2a) are employed as templates for the fabrication of bimetallic core-shell (CS) Au-Pd NPs, respectively, on the basis of the method reported in our previous work.[8,11]

Typically, 10 μL of 4-nitrophenol (4-NP, 10 mM), 2 mL of water, and 200 μL of $NaBH_4$ (0.1 M, freshly prepared, ice-cold) were added into a 10 mm path length quartz cuvette at room temperature, followed by the addition of the as-prepared CS Au-Pd NPs (Au_s-Pd NPs and Au_{dt}-Pd NPs) with a fixed number at about 10^{11} particles, to initiate the reaction (t=0). This reaction also can be easily monitored by UV-visible spectroscopy because 4-nitrophenolate ions and 4-aminophenol (4-AP) both display strong absorption peaks centered at 400 and 300 nm, respectively (Figure S17a and S17b).

To compare the catalytic activities of the Au_s-Pd NPs and Au_{dt}-Pd NPs, $\ln(A/A_0)$ is plotted as a function of reaction time, where A and A_0 are the relative concentrations of 4-NP at time t = t and t = 0, respectively (Figure S17c). In comparison with CS Au_s-Pd NPs with the comparable size, the CS Au_{dt}-Pd NPs showed a better performance in the hydrogenation catalysis of 4-NP. For instance, the reaction rate constant of CS Au_{dt}-Pd is reached up to 0.22 min^{-1}, which is higher than that of the Au_s-Pd NPs (0.15 min^{-1}) (Figure S17c), and much higher than that of the pure Pd NPs (0.14 min^{-1}) reported in the literature.[12]

Table S1. Summarized data of the volume of 3 nm Au-NP seeds (V_{seed}), the corresponding particle number of Au-NP seeds (N_{seed}), the concentrations of AA (n_{AA}) and Cu^{2+} ions (n_{cupric}) used for the preparation of differently-sized QS Au NPs.

Real diameter [nm]	V_{seed} [μL]	N_{seed}	n_{AA} [μM]	n_{cupric} [μM]
13	25	2.6×10^{12}	5	n/a
20	4	4.2×10^{11}	5	n/a
28	1.5	1.6×10^{11}	5	n/a
38	1	1.04×10^{11}	4.5	n/a
48	0.4	4.2×10^{10}	4.25	n/a
61	0.2	2.1×10^{10}	4	n/a
70	0.15	1.56×10^{10}	3.75 5	n/a 2
87	0.08	8.3×10^{9}	5	2
106	0.04	4.2×10^{9}	5	2
135	0.02	2.1×10^{9}	5	2
157	0.01	1.04×10^{9}	5	2
196	0.005	5.2×10^{8}	5	2

Note that in practical operation, the resulting solution of 3 nm Au-NP seeds were diluted from 10 to 10000 times before use. And the particle number concentration of 3 nm Au-NP seeds in the solution is about 1.04×10^{11} μL^{-1}. The amount of $HAuCl_4$ (10 mM, 0.25 mL) in the reaction media is fixed in all experiments.

Table S2. Summarized data of the real diameters, calculated diameters, size deviations, and ellipticities of the as-prepared QS Au_s NPs obtained by one-step seeded growth method in the absence of Cu^{2+} ions, the measured and calculated center positions of their SPR peaks.

Real diameter [nm]	Calculated diameter [nm]	Deviation [%] [a]	Ellipticity [b]	SPR mode	Exp. [nm] [c]	Mie [nm] [d]
13	13	6	1.05	dipo	521	521
20	24	5.4	1.05	dipo	521	521
28	33	3.9	1.06	dipo	524	521
38	38	3.9	1.05	dipo	524	524
48	52	4.4	1.05	dipo	528	529
61	66	4.6	1.05	dipo	534	533
70	74	2.6	1.04	dipo	548	545

Note: [a] The standard deviations of the real diameters of the as-prepared QS Au_s NPs are calculated on the basis of the statistical results of at least 100 particles; [b] Their ellipticities are estimated as the ratio of the major to minor axes; [c] The center positions of their SPR peaks measured by UV-vis spectroscopy; [d] The center positions of their SPR peaks calculated by using Mie theory.

Table S3. Calculated values of the angles of α, β, and γ of one TOH NP bounded by different crystallographic facets.

(hkl)	α	β	γ
(221)	141º	90º	141º
(331)	129.5º	102º	153.5º
(441)	124º	108º	160º

Table S4. Summarized SERS performance of CV probes adsorbed on the blank glass substrate, adsorbed on the glass substrates coated with 70 nm QS Au NPs with a rough surface, and adsorbed on the glass substrates coated with the 70 nm TOH Au NPs with sharp tips. The excitation laser wavelength for Raman measurements is 633 nm. The acquisition time is 10 s, and the laser power is 0.1 mW.

	I_{210}	EF_{210} [10^6]	Concentration of CV [M]
CV	197	None	None
QS Au NPs	2154	6.46	10^{-3}
TOH Au NPs	2794	3.85	
QS Au NPs	2411	7.23	10^{-5}
TOH Au NPs	3023	4.11	
QS Au NPs	3613	10.77	10^{-6}
TOH Au NPs	4612	6.26	
QS Au NPs	1691	5.06	10^{-7}
TOH Au NPs	3464	4.72	
QS Au NPs	600	1.78	10^{-8}
TOH Au NPs	1196	1.62	
QS Au NPs	390	1.17	10^{-9}
TOH Au NPs	939	1.28	

REFERENCES

1 Y. Song, T. Miao, P. Zhang, C. Bi, H. Xia, D. Wang and X. Tao, *Nanoscale*, 2015, **7**, 8405–8415.

2 E.C. Le Ru, E. Blackie, M. Meyer and P.G. Etchegoin, *J. Phys. Chem. C*, 2007, **111**, 13794–13803.

3 Q. Zhang, N. Large and H. Wang, *ACS Appl. Mater. Interfaces*, 2014, **6**, 17255–17267.

4 E. Nalbant Esenturk and A.R. Hight Walker, *J. Raman Spectrosc.*, 2009, **40**, 86–91.

5 V.O. Yukhymchuk, O.M. Hreshchuk, V.M. Dzhagan, M.V. Sakhno, M.A. Skoryk, S.R. Lavoryk, G.Y. Rudko, N.A. Matveevskaya, T.G. Beynik and M.Y. Valakh, *Phys. Status Solidi B*, 2019, **256**, 1800280.

6 T. Watanabe and B. Pettinger, *Chem. Phys. Lett.*, 1982, **89**, 501-507.

7 W.C. Lin, S.H. Huang, C.L. Chen, C.C. Chen, D.P. Tsai and H.P. Chiang, *Appl Phys A*, 2010, **101**, 185–189.

8 Y. Song, C. Xiang, C. Bi, C. Wu, H. He, W. Du, L. Huang, H. Tian and H. Xia, *Nanoscale*, 2018, **10**, 22302–22311.

9 H. Yildirim and A. Kara, *J. Phys. Chem. C*, 2013, **117**, 2893–2902.

10 M. Farmanbar and G. Brocks, *Phys. Rev. B*, 2016, **93**, 085304.

11 C. Wu, H. Li, H. He, Y. Song, C. Bi, W. Du and H. Xia, *ACS Appl. Mater. Interfaces*, 2019, **11**, 46902–46911.

12 K. Gu, X. Pan, W. Wang, J. Ma, Y. Sun, H. Yang, H. Shen, Z. Huang and H. Liu, *Small*, 2018, **14**, 1801812.